Optical Fiber Technology 18 (2012) 388–393

Contents lists available at SciVerse ScienceDirect

Optical Fiber Technology

www.elsevier.com/locate/yofte

# Quantitative coherent anti-Stokes Raman scattering microspectroscopy using a nanosecond supercontinuum light source

Masanari Okuno [a,1], Hideaki Kano [a,*], Philippe Leproux [b,c], Vincent Couderc [b,c], Hiro-o Hamaguchi [a,d]

[a] Department of Chemistry, School of Science, The University of Tokyo, 7-3-1 Hongo, Bunkyo-ku, Tokyo 113-0022, Japan
[b] Institut de Recherche XLIM, UMR CNRS 6172, 123 Avenue Albert Thomas, 87060 Limoges Cedex, France
[c] LEUKOS, ESTER Technopole, 1 Avenue d'Ester, 87069 Limoges Cedex, France
[d] Institute of Molecular Science and Department of Applied Chemistry, National Chiao Tung University, 1001 Ta Hsueh Road, Hsinchu 300, Taiwan

ARTICLE INFO

*Article history:*
Available online 27 June 2012

*Keywords:*
Raman
Coherent anti-Stokes Raman scattering
Microspectroscopy
Supercontinuum
Photonic crystal fiber
Spectral imaging
Living cell

ABSTRACT

We describe and characterize a multiplex CARS microspectroscopic system that uses a nanosecond supercontinuum generated from a photonic crystal fiber and a sub-nanosecond pulse laser. This system has a high spectral resolution (<0.1 $cm^{-1}$) and an ultrabroadband spectral coverage (>2500 $cm^{-1}$). The estimated spatial resolutions are 0.45 μm (lateral) and 4.5 μm (axial), respectively. This system enables us to obtain CARS spectra and corresponding images in the fingerprint region as well in the CH stretch region. Using this system, we have successfully obtained label-free and multi-mode vibrational images of a yeast cell.



## 1. Introduction

Vibrational spectroscopy, based on infrared (IR) absorption and Raman scattering, provides a powerful means for investigating biological samples at the molecular level. Vibrational spectra are highly sensitive to molecular structure and are often called the "molecular fingerprints". One promising application of vibrational spectroscopy is vibrational microscopy. In fact, vibrational microscopy attracts much attention these days as a chemical imaging tool with high vibrational specificity. Because of its noninvasive nature, vibrational microscopy has been applied extensively in life/biological sciences as well as in material sciences. For biological applications, Raman microscopy [1] is more advantageous than infrared microscopy in two aspects. First, Raman microscopy has higher spatial resolution than infrared due to the diffraction limit. Second, Raman spectroscopy is not seriously interfered by water, which has very strong absorption in the infrared region. Various linear and nonlinear optical techniques have been developed recently in order to promote Raman microscopy to become a practical tool for studying living systems. Among them, coherent anti-Stokes Raman scattering (CARS) microscopy is promising as a high-speed bioimaging tool [2,3]. CARS is one of the nonlinear Raman processes which provide vibrational spectral information [4]. In the CARS process, both the pump ($\omega_1$) and Stokes ($\omega_2$) laser pulses interact with a molecule. If the frequency difference between those two ($\omega_1 - \omega_2$) matches a vibrational frequency of the sample molecule ($\Omega$), a vibrational coherence is driven. Subsequently, this vibrational coherence is probed by the third laser pulse, giving rise to a strong CARS signal with frequency of $2\,\omega_1 - \omega_2$ (Fig. 1b). CARS is one-photon fluorescence free, since the wavelength of the CARS signal is blue-shifted from those of the incident laser pulses. Thus, CARS microscopy has the possibility to complement spontaneous Raman microscopy. In a past decade, CARS microscopy has made considerable progresses for high-speed molecular imaging [5–7]. However, current CARS microscopy using two narrow band laser pulses is not suitable for obtaining Raman spectra because it requires a sophisticated laser wavelength scanning technique. We cannot easily obtain full spectral information of molecules with conventional CARS microscopy.

In order to obtain Raman spectral information in a simple way, we have extended CARS microscopy to CARS microspectroscopy by using the multiplex CARS method. In the multiplex CARS process [8], we induce multiple vibrational coherences simultaneously by using a broadband light source as the Stokes pulse. By introducing the third pulse, we can obtain multiplex CARS spectra with multiple vibrational resonances. Thus, CARS microspectroscopy enables us to obtain a wealth of vibrational information of molecules without any elaborate scanning technique. Recently, a supercontinuum

* Corresponding author. Address: Institute of Applied Physics, University of Tsukuba, 1-1-1 Tennodai, Tsukuba, Ibaraki 305-8573, Japan.
*E-mail address:* hkano@bk.tsukuba.ac.jp (H. Kano).
[1] Present address: Max-Planck Institute for Polymer Research, Ackermannweg 10, 55128 Mainz, Germany.

1068-5200/$ - see front matter © 2012 Elsevier Inc. All rights reserved.
http://dx.doi.org/10.1016/j.yofte.2012.05.006

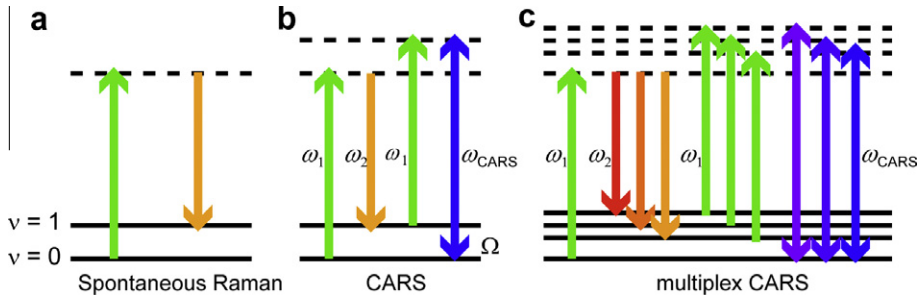


**Fig. 1.** Diagrams for spontaneous Raman scattering (a), CARS (b) and multiplex CARS process (c).

(SC) has been used as the Stokes laser for extending the spectral coverage of a CARS microspectrometer. The SC generated from the combination of a photonic crystal fiber (PCF) with a femtosecond (fs) or picosecond (ps) laser source is widely used in multiplex CARS microspectroscopy [9–14]. However, because of the large linewith of a fs or ps laser (typically, 10 $cm^{-1}$), the spectral resolution of CARS spectra is not enough to resolve the fingerprint region spectra (1800–800 $cm^{-1}$), where many bands are located close to one another. Very recently, a SC has become obtainable with the combination of a PCF with sub-nanosecond (sub-ns) microchip laser. This technique provides a low-cost, compact and ultrabroadband light source [15–19]. The linewidth of the pump laser (<0.1 $cm^{-1}$) is narrow enough to separate each band in the conjugated fingerprint region. In addition, the peak intensity of the ns laser is more than 10 times higher than that of a mode-lock ps laser with the same average power since the repetition rate of the ns laser (33 kHz) is much lower than that of a picosecond oscillator (typically in the order of 100 MHz). This high peak intensity is advantageous for generating a CARS signal efficiently. We have developed a multiplex CARS microspectrometer that employs this technique [20,21]. By using a nanosecond laser source as the pump radiation in the multiplex CARS process, we have greatly improved the spectral resolution of the system. Based on this system, we have developed quantitative CARS microspectroscopy with the use of the maximum entropy method (MEM) [21], polarization-resolved CARS microspectroscopy [22] and multi-modal imaging system including CARS, second harmonic generation, third harmonic generation and third sum frequency generation [23]. In this paper, we describe the details of the system that we have developed and its application to living cell studies.

## 2. Experimental

### 2.1. Methods

The schematic of our CARS microspectroscopic system is shown in Fig. 2a. A dual-output compact laser source has been used. The pump source is a passively Q-switched 1064-nm microchip laser. Typical temporal duration, repetition rate and average power are <1 ns, 33 kHz and ~300 mW, respectively. The fundamental laser beam is equally divided into two parts with a beam splitter. One part is directly used as the pump radiation (~5 kW peak power; ~150 mW average power; <0.1 $cm^{-1}$ linewidth) of the CARS process after adjusting its power with a variable neutral density filter. The other part is introduced into a 6-m-long air-silica PCF, characterized by a 2.5 μm hole diameter and a 4-μm hole-to-hole spacing, which result in a zero-dispersion wavelength of 1040 nm for

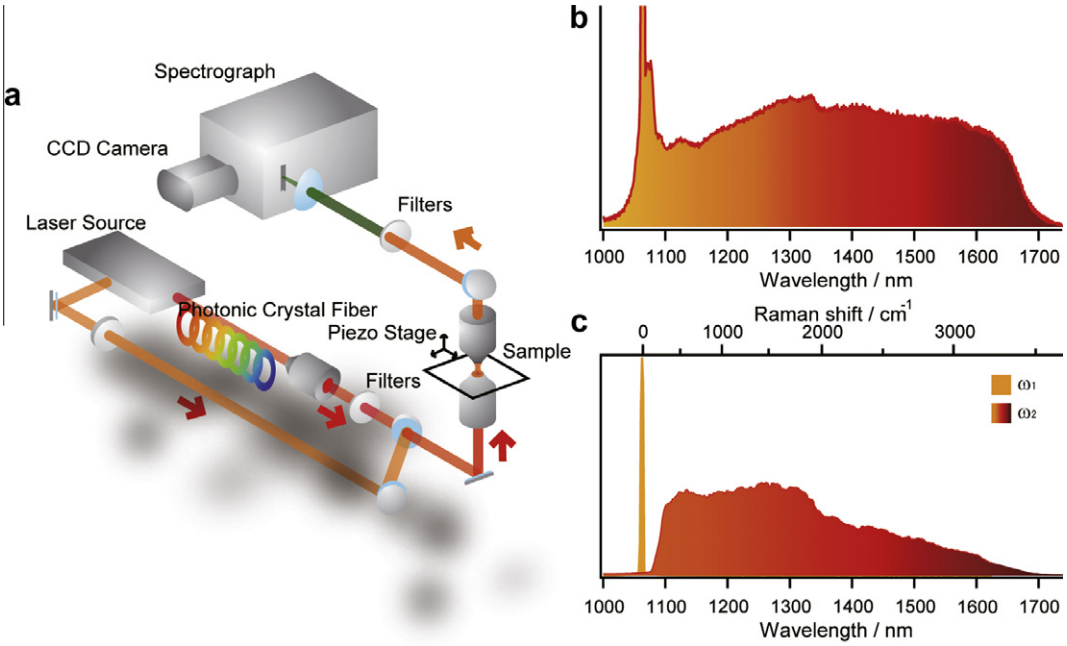


**Fig. 2.** (a) Schematics of our ultrabroadband multiplex CARS microspectrometer. (b) Typical spectrum of the white laser (linear scale). Note that the intensity at the 1064 nm is out of the vertical scale. (c) Typical spectra of the pump and Stokes laser pulses (linear scale).

the fundamental guided mode of the structure. The strong third-order nonlinear effects, that occur all along the propagation in the fiber, create white laser emission at the fiber output, with >100 μW/nm spectral power density from 1.05 μm to 1.6 μm. Fig. 2b shows a typical spectrum of the white laser. This white laser beam is used for the Stokes radiation of the CARS process. The pump and Stokes beams are passed through several filters to eliminate anti-Stokes spectral components, superimposed by a notch filter, and introduced into the modified inverted microscope (Nikon: ECLIPSE Ti). Typical spectral profiles of the pump and Stokes pulses are shown in Fig. 2c. The spectrum the Stokes pump covers a wide range of vibrational resonances (>3000 $cm^{-1}$) with the 1064 nm pump pulse. In a previous study, we showed that the Stokes light is well-defined in time-frequency domain [20]. The spectral distortion around 1.35 μm is due to the absorption of the overtone/combination of the OH stretch bands in the fiber and filters in the system. The pump and Stokes pulses are tightly focused onto the sample with an objective (Nikon: Plan Fluor 100×/NA 1.3). The CARS signal generated by the sample is collected by another objective (Nikon: Apo NIR 60×/NA 1.0) and guided into a spectrometer (Princeton Instruments: SpectraPro2300i and PIXIS 100BR). No precise delay line is needed in the setup since the temporal duration of both the pump and Stokes lasers are (sub-) nanosecond. The laser power of both the pump and Stokes lasers is 10 mW.

### 2.2. Materials

The sample was living fission yeast *Schizosaccharomyces pombe* (*S. pombe*). The cells were cultured in YE medium. For the preparation of samples of CARS microspectroscopic measurements, the growing cells and the YE broth were placed between cover glasses. The edge of the cover glass was sealed with Vaseline to prevent the volatilization of the medium. Because of a small quantity of the sample, yeast cells were immobilized. All measurements were performed at room temperature.

## 3. Results and discussion

Fig. 3a shows an intensity-corrected multiplex CARS spectrum of crystalline L-cystine. The molecular structure of L-cystine is shown in Fig. 3b. The intensity correction has been carried out using the nonresonant background signal of an underneath cover glass measured under the same experimental condition. The CARS spectrum gives a slightly dispersive line shape due to the interference with the nonresonant background. The CARS spectrum of L-cystine shows many peaks due to various Raman resonances. The intense peaks around 2965 $cm^{-1}$, 2910 $cm^{-1}$ and 500 $cm^{-1}$ originate from the $CH_3$ degenerate stretch, the $CH_3$ symmetric stretch and the disulfide bond stretch (S—S), respectively. In addition, the spectral profile in the fingerprint region is obtained simultaneously (the inset of Fig. 3a). All the sharp features in the inset of Fig. 3a originate from vibrational resonances. Thus, simultaneous detection of all the CARS signals between 500 $cm^{-1}$ and 3000 $cm^{-1}$ is performed with high spectral resolution. The spectral resolution is determined not by the laser linewidth but by the dispersion of the polychromator.

Fig. 4a shows the CARS intensity dependence curve of the 1310 $cm^{-1}$ Raman band ($NO_2$ symmetric stretch) at the edge of an N, N-dimethyl-para-nitroaniline crystal. By fitting this curve with a step function convoluted with a Gaussian, we determined the full width at half-maximum to be 0.45 μm. Fig. 4b shows the depth dependence of the CARS signal of liquid ethanol at 883 $cm^{-1}$ (the C—C stretch), which is measured across the interface between the cover glass and the liquid. The intensity profile is fitted well with a step function convoluted with a Gaussian. From the fitting, the axial spatial resolution of the present CARS microspectrometer is estimated to be 4.5 μm.

Fig. 5a–c shows three CARS spectra in the CH stretch region obtained from three different positions in a living cell. They give highly dispersive line shapes due to the interference between the CARS and the nonresonant background signals. We employ the maximum entropy method (MEM) to extract the amplitude and phase of vibrational resonances from the complicated CARS spectra [24,25] that we observe. The MEM does not require any a priori information about the vibrational bands but still is able to retrieve the phase information on the third-order nonlinear susceptibility of the CARS process, $\chi^{(3)}$. The imaginary part of $\chi^{(3)}$, $\mathrm{Im}[\chi^{(3)}]$, corresponds to a spontaneous Raman spectrum, whose intensity is proportional to molecular concentration. Fig. 5d–f shows the $\mathrm{Im}[\chi^{(3)}]$ spectra converted by MEM from the observed multiplex CARS spectra in Fig. 5a–c, respectively. The dispersive line shapes in Fig. 5a–c are successfully converted into the band shapes similar to spontaneous Raman spectra. Subsequently, we employed a singular value decomposition analysis to reduce the noise in the $\mathrm{Im}[\chi^{(3)}]$ spectra [26]. The results are shown in Fig. 5g–i. The signal-to-noise ratio (SNR) is considerably improved compared with the $\mathrm{Im}[\chi^{(3)}]$ spectra in Fig. 5d–f.

We now discuss the $\mathrm{Im}[\chi^{(3)}]$ spectra in Fig. 5g–i. The spectrum in Fig. 5g shows the intense and sharp $CH_2$ signal at 2850 $cm^{-1}$, which originates from lipid molecules. On the other hand, both

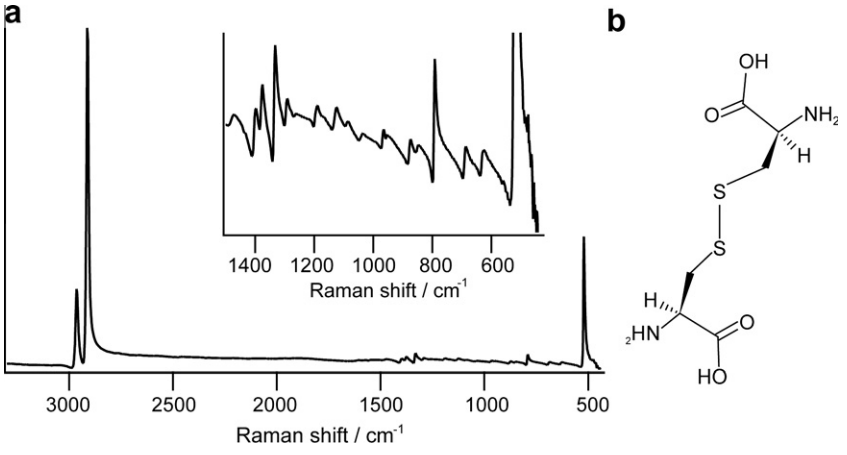


**Fig. 3.** (a) An intensity-corrected CARS spectrum of L-cystine. The inset is the expanded spectrum in the fingerprint region (linear scale). (b) The molecular structure of L-cystine.

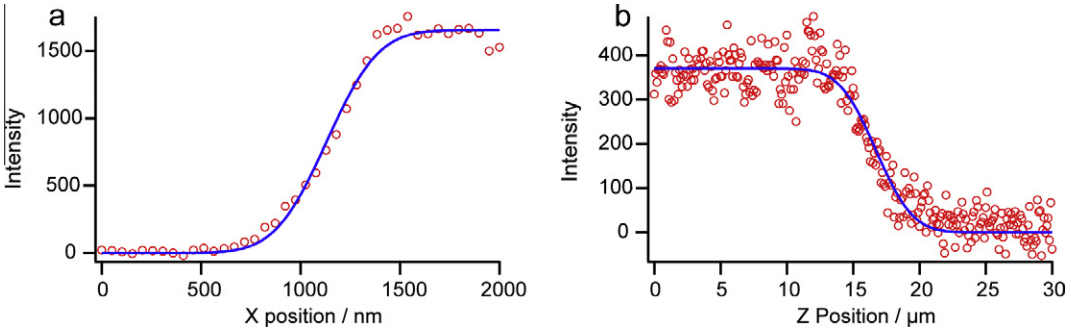


**Fig. 4.** CARS intensity profiles of N, N-para-nitroaniline in lateral (a) and of ethanol in axis (b) (linear scale).

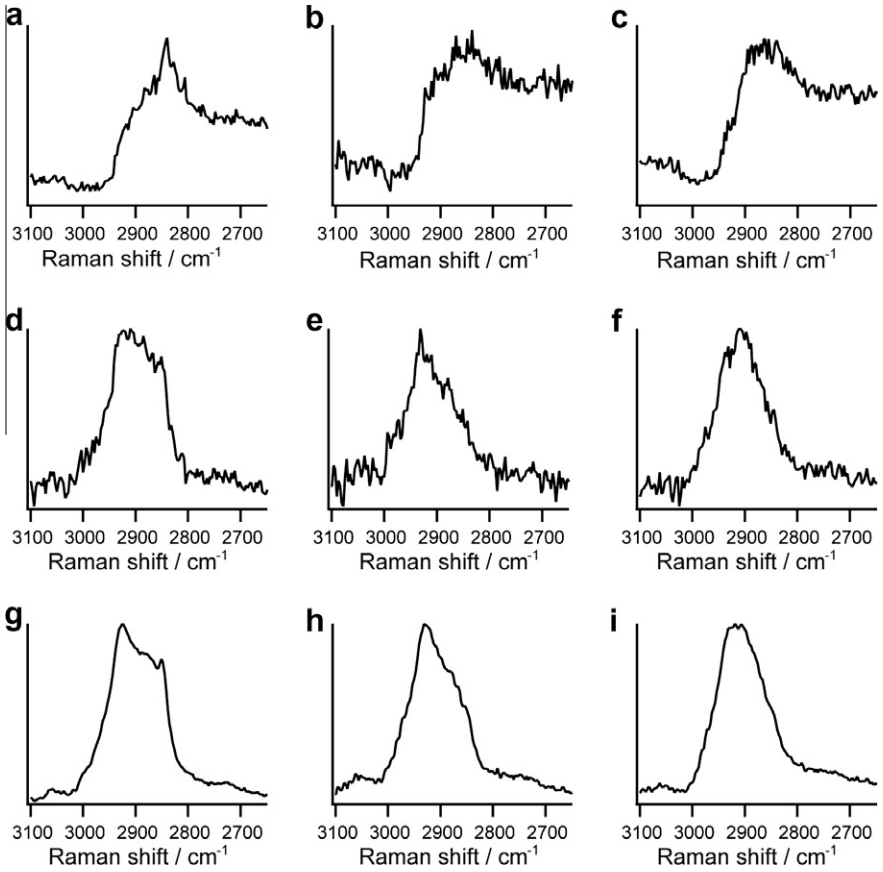


**Fig. 5.** (a-c) Typical CARS spectra in the CH stretch region of a living yeast cell, (d-f) Im[$\chi^{(3)}$] spectra obtained by MEM, (g-i) Im[$\chi^{(3)}$] spectra after a SVD analysis. All the spectra are plotted in a linear scale.

of the Im[$\chi^{(3)}$] spectra in Fig. 5h and i show strong $CH_3$ signals. Considering the fact that proteins have a larger $CH_3/CH_2$ ratio than lipids, we conclude that these spectra are obtained from a protein rich part of the cell. The spectra in Fig. 5h and i look similar to each other but show a slight difference of the band shape, reflecting the difference of chemical compositions between the two positions. Furthermore, our quantitative CARS technique enables us to observe relatively small bands in this region, the bands around 2730 $cm^{-1}$ (CH stretch) and 3050 $cm^{-1}$ (C═C—H stretch), which are not detectable in usual CARS microscopy. Thus, even in the CH stretch region, CARS microspectroscopic approach enables us to obtain much more detailed vibrational information than that obtainable from CARS microscopy.

We are able to observe the multiplex CARS spectra in the fingerprint region simultaneously. Fig. 6a–c shows three fingerprint region CARS spectra from the three positions, where Fig. 5a–c are obtained, respectively. We employ the same MEM and SVD analysis. The results are shown in Fig. 6d–f and g–i, respectively. The dispersive CARS spectra with a low SNR are converted to Im[$\chi^{(3)}$] spectra with a high SNR by the MEM and SVD. By comparison with our previous spontaneous Raman study [27], the overall spectral features of the spectrum in Fig. 6g is measured from a lipid rich part and Fig. 6h and i from a protein rich part of the cell. This is consistent with the discussion for the CH stretch region given above. The broadband spectral profile around 1100 $cm^{-1}$ in Fig. 6i is similar to the polysaccharide such as mannan and β-1,3-glucan, contained in a matured septum of a cell.

Fig. 7 shows label-free and multi-mode (9 frequencies) Im[$\chi^{(3)}$] images of a living yeast cell. Peak intensities of Im[$\chi^{(3)}$] spectra are used for constructing these images. The exposure time for each

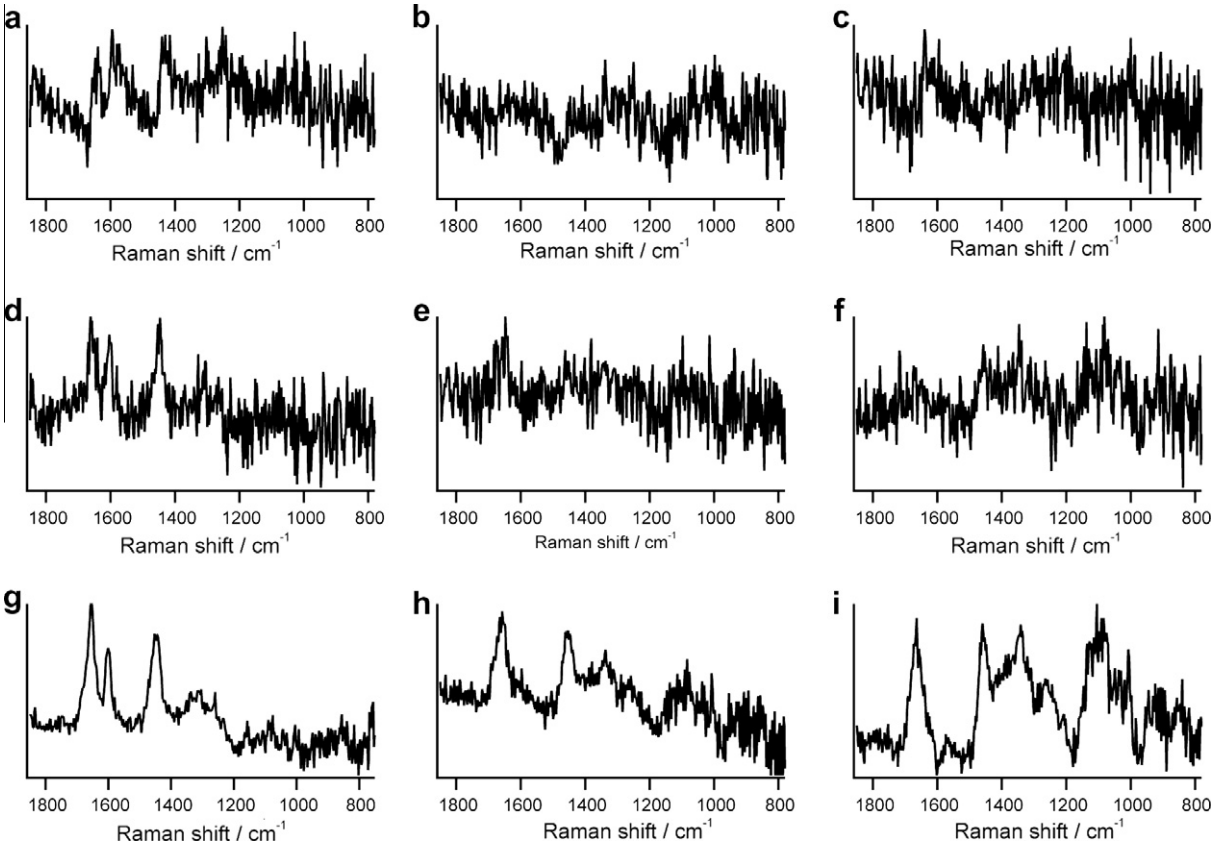


**Fig. 6.** CARS spectra in the fingerprint region corresponding to Fig. 4, (d–f) Im[$\chi^{(3)}$] spectra obtained by MEM, (g-i) Im[$\chi^{(3)}$] spectra after a SVD analysis. All the spectra are plotted in a linear scale.

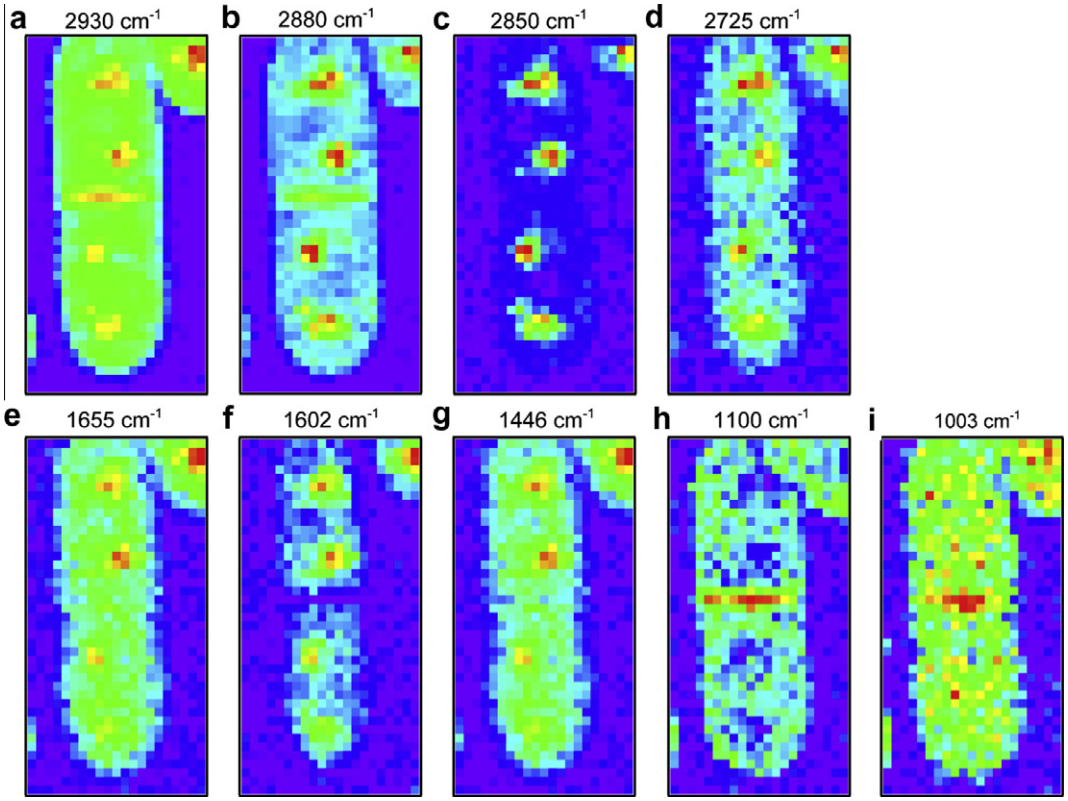


**Fig. 7.** Label-free and multi-frequency (9 frequencies) Im[$\chi^{(3)}$] images of a living yeast cell at the Raman shift of 2930, 2880, 2850, 2725, 1665, 1602, 1446, 1100, 1003 $cm^{-1}$ (a–i).

pixel is 50 ms and each image consists of 21 × 41 pixel. The overall acquisition time is 45 s. The intense CH stretch band around 2880 $cm^{-1}$ is decomposed into three, the $CH_3$ stretch (2930 $cm^{-1}$), $CH_2$ stretch (2850 $cm^{-1}$) and these superposition (around 2880 $cm^{-1}$) by fitting the CARS spectra with a sum of three Lorentzian. The Raman bands at 1665, 1446, and 1003 $cm^{-1}$ are assigned to the lipid C=C stretch/the protein amide I, the CH bend and phenylalanine residues. The Raman band at 1602 $cm^{-1}$ is called the "Raman spectroscopic signature of life" by us, sharply reflecting the metabolic activity of a yeast cell [27,28]. We can classify the Im[$\chi^{(3)}$] images into four groups. The first group consists of the images in Fig. 7c, d, and f. They show localized and intense signals inside the cell. The images of this group are ascribed to lipid molecules, probably contained in lipid droplets. The second one is the image in Fig. 7i. The image shows a homogeneous distribution. Since the Raman band at 1003 $cm^{-1}$ is assigned to the phenylalanine residues, this image most probably reflects the distribution of proteins inside the cell. The third one is the images in Fig. 7a, e, and g. They look like the sum of images in the first and second group. This result is consistent with the band assignments. The Raman signals giving the images in this category are found not only for lipid molecules but also for proteins. The fourth one is the image in Fig. 7h. The image shows relatively localized signal at the middle of the cell. Since the broad Raman band at 1100 $cm^{-1}$ is assigned to polysaccharides, the intense signal at the middle of the cell reflects the matured septum of the cell. The images in Fig. 7a and i also show strong signals at the middle of the cell but the images in Fig. 7c and f show no signal there. This fact suggests that the matured septum contains abundant proteins and small quantity of lipid molecules. Our previous CARS study on a fission yeast cell [12] was unable to detect such minute differences of chemical compositions of the septum because of its low spectral resolution.

## 4. Conclusion

We have described the details of our CARS microspectrometer giving its spectral resolution, spectral coverage and spatial resolutions. A nanosecond SC generated from a PCF combined with a subnanosecond microchip laser has improved the spectral resolution and extended the spectral coverage considerably. By using this system, we have successfully obtained vibrational spectra and images of a living cell. Multiplex CARS microspectroscopy using a nanosecond SC will find extensive applications not only in life/biological sciences but also in other fields including material sciences.

## Acknowledgments

This work is supported by the SENTAN project (Program-S) of the Japan Science and Technology Agency (JST). H. Kano gratefully acknowledges financial support by, Grand-Aid for Scientific Research on Priority Areas "Molecular Science for Supra Functional Systems" [477] from MEXT, and the Global COE Program for "Chemistry Innovation". The authors gratefully acknowledge J. Ukon, HORIBA, Ltd. for assisting a fruitful collaboration between Japanese and French labs.

## References

[1] G.J. Puppels, F.F.M. Demul, C. Otto, J. Greve, M. Robertnicoud, D.J. Arndtjovin, T.M. Jovin, Studying single living cells and chromosomes by confocal Raman microspectroscopy, Nature 347 (1990) 301–303.
[2] M.D. Duncan, J. Reintjes, T.J. Manuccia, Scanning coherent anti-Stokes Raman microscope, Opt. Lett. 7 (1982) 350–352.
[3] A. Zumbusch, G.R. Holtom, X.S. Xie, Three-dimensional vibrational imaging by coherent anti-Stokes Raman scattering, Phys. Rev. Lett. 82 (1999) 4142–4145.
[4] M.D. Levenson, S. Kano, Introduction to Nonlinear Laser Spectroscopy, Academic Press, Boston, 1988.
[5] J.X. Cheng, L.D. Book, X.S. Xie, Polarization coherent anti-Stokes Raman scattering microscopy, Opt. Lett. 26 (2001) 1341–1343.
[6] J.X. Cheng, A. Volkmer, L.D. Book, X.S. Xie, An epi-detected coherent anti-Stokes Raman scattering (E-CARS) microscope with high spectral resolution and high sensitivity, J. Phys. Chem. B 105 (2001) 1277–1280.
[7] E.O. Potma, C.L. Evans, X.S. Xie, Heterodyne coherent anti-Stokes Raman scattering (CARS) imaging, Opt. Lett. 31 (2006) 241–243.
[8] B.N. Toleutaev, T. Tahara, H. Hamaguchi, Broadband (1000 $cm^{-1}$) multiplex CARS spectroscopy – application to polarization-sensitive and time-resolved measurements, Appl. Phys. B – Lasers Opt. 59 (1994) 369–375.
[9] T.W. Kee, M.T. Cicerone, Simple approach to one-laser, broadband coherent anti-Stokes Raman scattering microscopy, Opt. Lett. 29 (2004) 2701–2703.
[10] H. Kano, H. Hamaguchi, Vibrationally resonant imaging of a single living cell by supercontinuum-based multiplex coherent anti-Stokes Raman scattering microspectroscopy, Opt. Exp. 13 (2005) 1322–1327.
[11] G.I. Petrov, R. Arora, V.V. Yakovlev, X. Wang, A.V. Sokolov, M.O. Scully, Comparison of coherent and spontaneous Raman microspectroscopies for noninvasive detection of single bacterial endospores, Proc. Natl. Acad. Sci. USA 104 (2007) 7776–7779.
[12] H. Kano, H. Hamaguchi, Supercontinuum dynamically visualizes a dividing single cell, Anal. Chem. 79 (2007) 8967–8973.
[13] M.S.A. Courjaud, E. Mottay, C. Finot, J. Dudley, H. Rigneault, Polarized multiplex coherent anti-Stokes Raman scattering using a picosecond laser and a fiber supercontinuum, J. Biomed. Opt. 16 (2011) 021108.
[14] E.R. Andresen, H. Rigneault, Soliton dynamics in photonic-crystal fibers for coherent Raman microspectroscopy and microscopy, Opt. Fiber Technol. (2012).
[15] L. Provino, J.M. Dudley, H. Maillotte, N. Grossard, R.S. Windeler, B.J. Eggleton, Compact broadband continuum source based on microchip laser pumped microstructured fibre, Electron. Lett. 37 (2001) 558–560.
[16] S.G. Leon-Saval, T.A. Birks, W.J. Wadsworth, P.S.J. Russell, M.W. Mason, Supercontinuum generation in submicron fibre waveguides, Opt. Exp. 12 (2004) 2864–2869.
[17] W.J. Wadsworth, N. Joly, J.C. Knight, T.A. Birks, F. Biancalana, P.S.J. Russell, Supercontinuum and four-wave mixing with Q-switched pulses in endlessly single-mode photonic crystal fibres, Opt. Exp. 12 (2004) 299–309.
[18] P.A. Champert, V. Couderc, P. Leproux, S. Fevrier, V. Tombelaine, L. Labonte, P. Roy, C. Froehly, P. Nerin, White-light supercontinuum generation in normally dispersive optical fiber using original multi-wavelength pumping system, Opt. Exp. 12 (2004) 4366–4371.
[19] V. Tombelaine, C. Lesvigne, P. Leproux, L. Grossard, V. Couderc, J.L. Auguste, J.M. Blondy, G. Huss, P.H. Pioger, Ultra wide band supercontinuum generation in air-silica holey fibers by SHG-induced modulation instabilities, Opt. Exp. 13 (2005) 7399–7404.
[20] M. Okuno, H. Kano, P. Leproux, V. Couderc, H. Hamaguchi, Ultrabroadband multiplex CARS microspectroscopy and imaging using a subnanosecond supercontinuum light source in the deep near infrared, Opt. Lett. 33 (2008) 923–925.
[21] M. Okuno, H. Kano, P. Leproux, V. Couderc, J.P.R. Day, M. Bonn, H. Hamaguchi, Quantitative CARS molecular fingerprinting of single living cells with the use of the maximum entropy method, Angew. Chem., Int. Ed. 49 (2010) 6773–6777.
[22] K. Bito, M. Okuno, H. Kano, S. Tokuhara, S. Naito, Y. Masukawa, P. Leproux, V. Couderc, H. Hamaguchi, Protein secondary structure imaging with ultrabroadband multiplex coherent anti-Stokes Raman scattering (CARS) microspectroscopy, J. Phys. Chem. B 116 (2012) 1452–1457.
[23] H. Segawa, M. Okuno, H. Kano, P. Leproux, V. Couderc, H. Hamaguchi, Label-free tetra-modal molecular imaging of living cells with CARS, SHG, THG and TSFG (coherent anti-Stokes Raman scattering, second harmonic generation, third harmonic generation and third-order sum frequency generation), Opt. Exp. 20 (2012) 9551–9557.
[24] E.M. Vartiainen, K.E. Peiponen, T. Tsuboi, Analysis of coherent Raman-spectra, J. Opt. Soc. Am. B – Opt. Phys. 7 (1990) 722–725.
[25] E.M. Vartiainen, H.A. Rinia, M. Muller, M. Bonn, Direct extraction of Raman line-shapes from congested CARS spectra, Opt. Exp. 14 (2006) 3622–3630.
[26] H.J. van Manen, Y.M. Kraan, D. Roos, C. Otto, Intracellular chemical imaging of heme-containing enzymes involved in innate immunity using resonance Raman microscopy, J. Phys. Chem. B 108 (2004) 18762–18771.
[27] Y.S. Huang, T. Karashima, M. Yamamoto, H. Hamaguchi, Molecular-level investigation of the structure, transformation, and bioactivity of single living fission yeast cells by time- and space-resolved Raman spectroscopy, Biochemistry 44 (2005) 10009–10019.
[28] Y.S. Huang, T. Karashima, M. Yamamoto, T. Ogura, H. Hamaguchi, Raman spectroscopic signature of life in a living yeast cell, J. Raman Spectrosc. 35 (2004) 525–526.